THE ANNALS OF "DUNĂREA DE JOS" UNIVERSITY OF GALAȚI
FASCICLE V, TECHNOLOGIES IN MACHINE BUILDING,
ISSN 1221- 4566, 2009

NEWTECH 2009, GALATI

EFFECTS OF FINITE ELEMENT TYPE ON SPRINGBACK SIMULATION OF A HIGH STRENGTH STEEL SHEET

Takayuki HAMA[1,2], Mihaela BANU[3]

[1]Graduate school of Energy Science, Kyoto University, Japan
[2]Volume-CAD System Research Program, RIKEN, Japan
[3] Department of Manufacturing Science and Engineering, University of Galati, Romania
email: hama@energy.kyoto-u.ac.jp

ABSTRACT

Effects of finite element type on springback simulation of a high strength steel sheet are investigated using isotropic and combined hardening models. Solid and shell elements are used to model a DP600 steel sheet and the differences in the stress field during a two-dimensional draw-bending process are examined. The amount of springback tends to decrease by taking kinematic hardening into account, but this trend tends to invert, i.e. the sprigback tends to increase, as the initial tensile stress is increased. This inversion arises at much lower initial tensile stress when shell element is used compared to solid element. Reasons of the difference shown between solid and shell elements are investigated in terms of evolutions and distributions of stress components.

KEYWORDS: sheet metal forming, springback, finite element method, static explicit method, kinematic hardening.

1. INTRODUCTION

Springback is a critical defect in sheet metal forming and its compensation needs much time. Although numerical prediction using finite element method (FEM) is a powerful tool to predict mechanical behaviours of metal sheets, the prediction accuracy of final stress field is still improvable [1-4]. In our previous paper [5] two significantly different FEM codes – a static implicit code DD3IMP [2, 6] using solid elements and a static explicit code STAMP3D [1, 7] using shell elements – were used to simulate a two-dimensional draw-bending process of a DP600 steel sheet, and the results were compared especially focusing on stress evolutions. It was found that effects of kinematic hardening on the stress evolutions were notably different between the two codes. We concluded in the previous paper that this difference was due to the difference of finite element type used, i.e. solid and shell elements. Because differences between the two codes are not only the finite element type but also a time-marching scheme and a contact treatment, it is difficult to clearly specify origins of the difference shown in the stress evolutions.

In this paper, we carry out similar comparisons between solid and shell elements using only STAMP3D and the differences in the stress field as well as springback are investigated in detail.

2. STATIC EXPLICIT CODE STAMP3D

The static explicit elastoplastic FEM code STAMP3D [1, 7] was used in this study. STAMP3D utilizes the updated Lagrangian rate formulation to describe the finite deformation problem. Assuming that the rate-form relation is preserved during a small time increment Δt, all rate quantities can simply be replaced by incremental quantities as

$$\Delta \overset{\circ}{\tau}_{(J)} = \overset{\circ}{\tau}_{(J)} \Delta t,\ \Delta f = \dot{f} \Delta t,\ \Delta L = L \Delta t, \quad (1)$$

where $\overset{\circ}{\tau}_{(J)}$ is the Jaumann rate of the Kirchhoff stress tensor, f is the surface traction vector prescribed on the boundary of the domain, and L is the velocity gradient tensor. The generalized r_{min}-strategy [8] is used to limit the size of the increment to preserve the approximate linearity during the increment. However, the nodal equilibrium between the external and internal forces at the end of increment is not guaranteed because of the tangent solution employed. To overcome the difficulty, an explicit algorithm ALGONEQ [9] is employed in order to systematically

cancel the residual non-equilibrated nodal forces whenever their norm exceeds a prescribed admissible tolerance. The elastoplastic material behaviour is assumed to be isotropic small-strain elasticity and orthotropic large-deformation plasticity. Hill's quadratic yield function and the associated flow rule are used. Tools are assumed rigid and their surfaces are represented by a set of the so-called Nagata patch [1, 10-13].

3. SIMULATION CONDITIONS

3.1. Draw bending process

Simulations of a two-dimensional draw-bending process [1] of a dual-phase steel sheet were carried out. The simulation conditions were determined after our previous study [5]. Figure 1 shows the geometry of the tools. The blank was 5 mm wide, 200 mm long and 1 mm thick. Owing to the geometrical and material symmetries of the process, only half of the part was modelled. For simplicity, the plane strain condition was assumed in the width direction, to which corresponding boundary conditions were given. The blank was modelled either by eight-node solid elements with selective reduced integration or by four-node degenerated shell elements with assumed-strain field (ASF) integration [14]. The numbers of elements along the width and longitudinal directions were 1 and 100, respectively. Through thickness direction, the blank was discretized with 4 elements in case of solid elements, while eight Gauss integration points were given in case of shell elements.

Friction was not taken into account. However, an "equivalent to friction" stretching force was initially imposed to the blank edge in order to substitute and simulate the behaviour of the blankholder during the forming process. In short, calculation procedures adopted in the present draw bending simulation consisted of the following three stages. In the first stage, the tensile nodal forces were applied on the blank edge until a prescribed longitudinal stress is reached. In the second stage the blank was drawn until a punch stroke of 70 mm. In the third stage the springback calculation was carried out. The amount of springback was evaluated by the sidewall curvature.

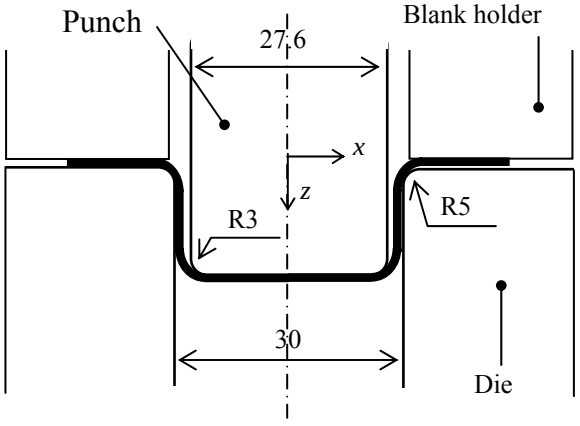

Figure 1. Tool geometries in mm.

3.2. Material model

A DP600 dual-phase steel was chosen for the present analysis. Two constitutive models were considered: isotropic hardening described by Swift, with or without considering a non-linear kinematic hardening (KH) law with saturation. Hill's 48 yield criterion was used. The constitutive parameters identified within LPMTM-CNRS, France [15] are shown in Table 1. In the remaining of this paper, following notations are used: Swift – Swift without KH, SKH – Swift plus KH.

Table 1 Material parameters used in the simulation

Hardening Law	Identified parameters
Swift	Y_0 = 330.0 MPa, C = 1093.0 MPa, n = 0.187
Swift + Kinematic Hardening	Y_0 = 308.3 MPa, C = 790.2 MPa, n = 0.132, C_x=15.8, X_{sat}= 169.2MPa
Hill'48 Yield Criterion	F = 0.490, G = 0.504, H = 0.496, N = 1.27 r_0=1.01, r_{45} =0.76, r_{90}=0.98

4. SIMULATION RESULTS

Figure 2 shows the evolution with the punch stroke of the longitudinal stress at the Gauss point "*a*" on the die-side of the cross section, which is identified schematically on Fig. 2. This result is obtained with shell elements, the initial tensile stress of 40 MPa, and Swift. The point *a* comes at the die shoulder at a punch stroke of about 17 mm, and is then subjected to bending and unbending. After experiencing unbending at a punch stroke of about 30 mm, the longitudinal stress starts decreasing at the sidewall and this trend is maintained until the end of the process. Although this overall trend is the same irrespective of the simulation conditions, large differences are observed in the amount of stress decrease at the sidewall depending on the simulation conditions. Because the amount of springback is generally determined by the final stress field, the difference in the stress decrease may result in the difference in the amount of springback. To see this correlation in detail, the amount of stress decrease $\Delta\sigma$ is defined as shown in Fig. 2 and its variations with the initial tensile stress are examined in Fig. 3 (a). In case of solid element, $\Delta\sigma$ obtained with Swift is always larger than that with SKH although the difference between Swift and SKH tends to decrease as increasing the initial tensile stress. In case of

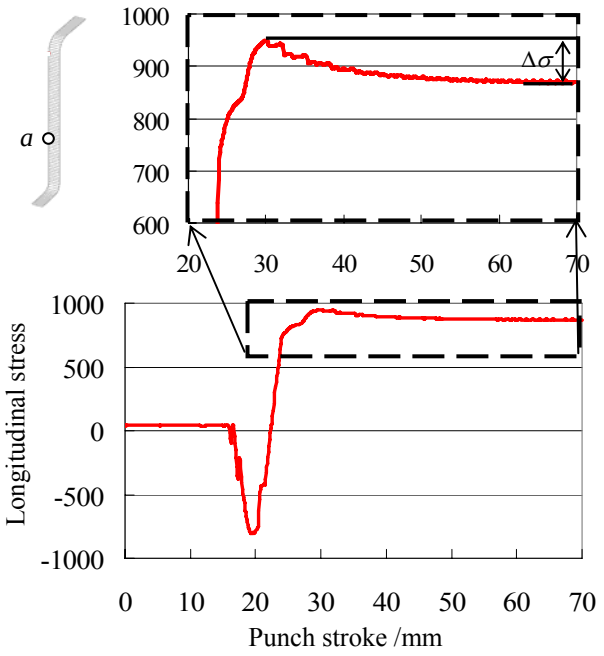

Figure 2 Longitudinal stress evolution at the integration point *a* on the die-side of the cross-section. Upper figure shows a zoom in the range of the punch stroke between 20 – 70 mm.

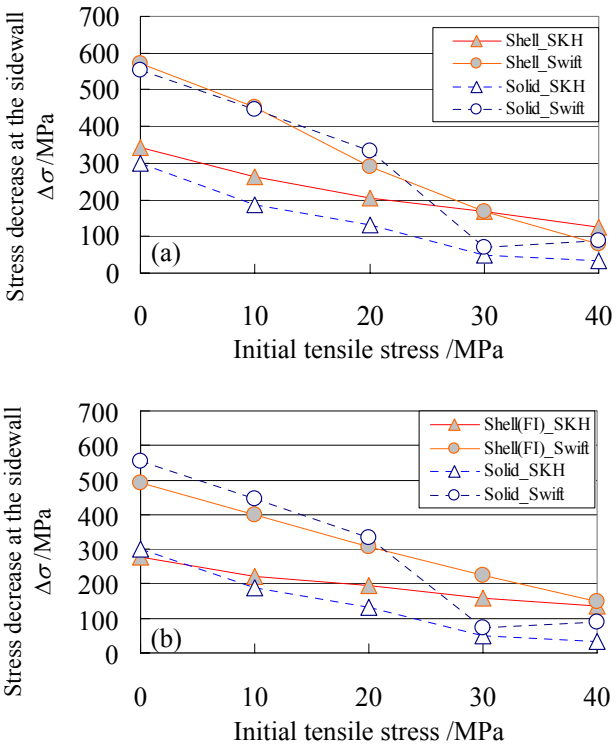

Figure 3 Relationships between initial tensile stress and stress decrease at the sidewall. (a) Results obtained with shell element with ASF and solid element, and (b) results obtained with shell elements with FI and solid element.

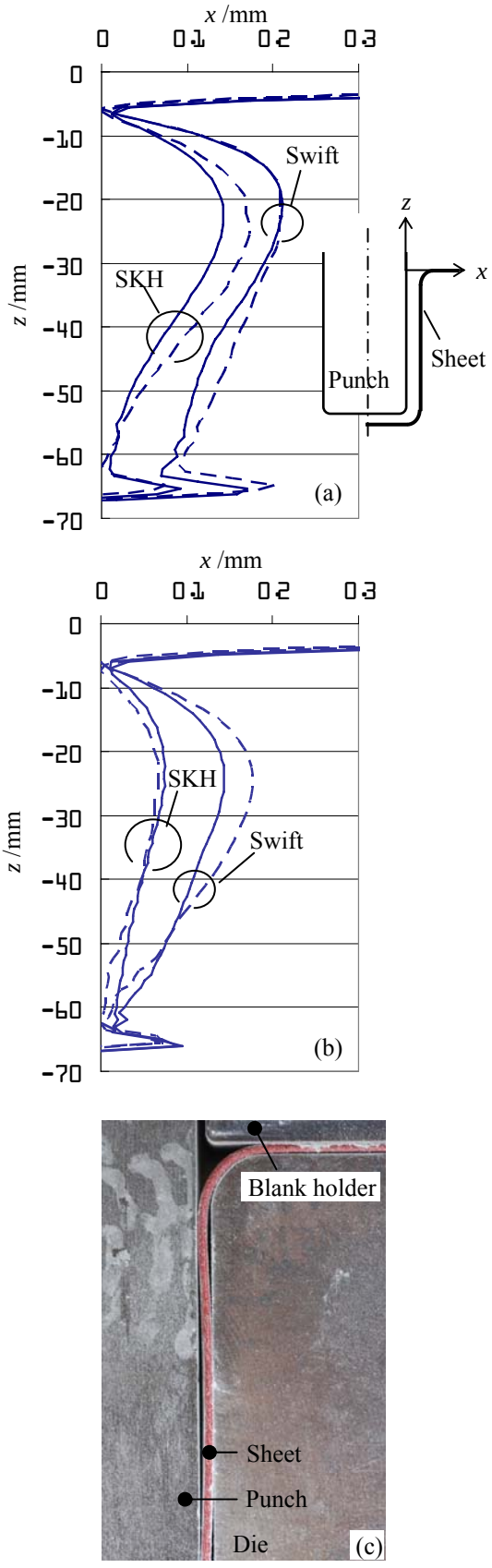

Figure 4. Deformed profiles at the sidewall before springback. Solid and dotted lines are the results of shell and solid elements, respectively. Initial tensile stresses are (a) 0 MPa, and (b) 20 MPa. (c) Photograph of the reverse bending.

shell element, on the other hand, the result obtained with Swift is relatively in good agreement with that obtained by solid element, whereas the gradient of the stress decrease with respect to the initial tensile stress obtained with SKH is more gradual than that obtained by solid element. Eventually the trend between Swift and SKH inverts beyond an initial tensile stress of 30 MPa.

It is known that this stress decrease is due to the so-called over-run phenomenon [1], which is the deformation at the sidewall that the sheet contacts the sidewall of the punch and hence is subjected to reverse bending. Figure 4 shows the deformed profiles at the sidewall before springback for the initial tensile stresses of 0 and 20 MPa. A photograph of the reverse bending obtained from an experiment is also shown for reference. The reverse bending apparently arises in all the results, but its magnitude is different depending on the simulation conditions. The reverse bending obtained with the initial tensile stress of 20 MPa is smaller than that of 0 MPa. Moreover the reverse bending obtained with Swift is larger than that of SKH. These trends are in good agreement with those observed in the stress decrease.

Next the relationship between the initial tensile stress and the sidewall curvature is shown in Fig. 5 (a). The sidewall curvature increases as the initial tensile stress increases irrespective of the simulation conditions. This is due to the fact that $\Delta\sigma$ decreases as the initial tensile stress increases as shown in Fig. 3 (a) and hence the amount of elastic recovery increases. In case of shell element, the sidewall curvature obtained with SKH is larger than that with Swift for the low initial tensile stress, whereas the trend inverts for the high initial tensile stress. However, such trend is much less obvious in case of solid element. Clearly the stress decrease correlates highly with the amount of springback, i.e. the sidewall curvature. These results show that the amount of springback basically tends to decrease by taking kinematic hardening into account, but this trend tends to invert when the initial tensile stress, i.e., the friction force due to the blank holding force, is increased. Moreover this inversion arises at much lower initial tensile stress in case of shell element compared to solid element. Therefore the differences between solid and shell elements observed in our previous study [5] are presumably due to the fact that the comparisons in our previous paper was carried out after the trends for shell elements inverted.

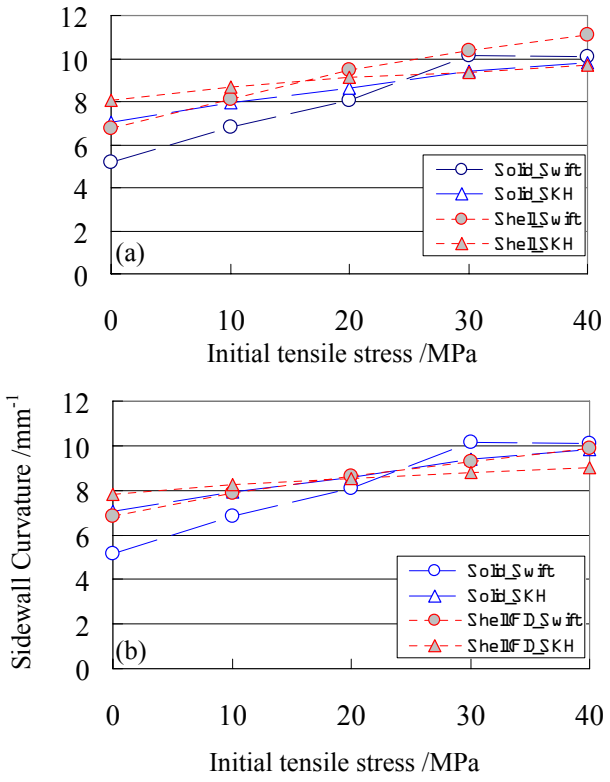

Figure 5 Relationships between the initial tensile stress and the sidewall curvature. (a) Results obtained by shell element with ASF and solid element, and (b) Results obtained by shell element with FI and solid element.

5. DISCUSSION

As discussed above, the inversions in the trend

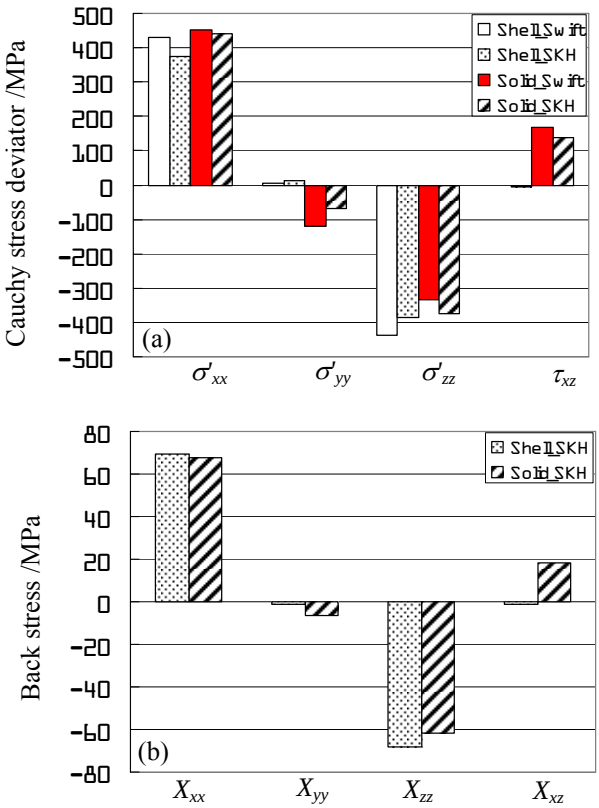

Figure 6 Stress components before springback obtained with shell element with ASF and solid element for an initial tensile stress of 40 MPa. (a) Cauchy stress deviator $\boldsymbol{\sigma}'$, and (b) back stress $\boldsymbol{X}$. The subscripts x, y and z denote the longitudinal, width, and thickness directions, respectively.

are much more obvious for shell element than for solid element. To investigate origins of the differences in the trend, Fig. 6 shows the Cauchy stress deviator and back stress components σ' and X at the point "*a*" before springback, i.e., at a punch stroke of 70 mm. The results obtained with an initial tensile stress of 40 MPa are shown. It is noted that the stress components are in the material frame where *x*, *y*, and *z* denote respectively the longitudinal, width, and thickness directions, and the components negligibly small are not presented here. Although the normal stress components are in good agreement irrespective of the simulation conditions, large differences are observed between shell and solid elements in the out-of-plane shear components τ_{xz} and X_{xz}. Clearly, these components obtained with shell element are much smaller than those with solid element. This result is due to the fact that the shell element with ASF employed in this study evaluates shear components small in order to overcome the shear locking problem. To examine effects of the out-of-plane shear components on the stress decrease, similar calculations are carried out using a shell element with full integration (FI) with which the shear components are also fully integrated. The results obtained by shell element with FI are shown in Figs. 3 (b), 5 (b) and 7. As shown in Fig. 7, not only the normal components but also the shear components obtained by shell element with FI are in good agreement with those obtained by solid element. However, as shown in Figs. 3 (b) and 5 (b), the trends of the stress decrease and the springback obtained by shell element with FI are rather closer to that obtained by shell element with ASF and the trend tends to invert at the high initial tensile stresses. These results show that the differences in the out-of-plane shear components are not a critical factor for the difference observed between solid and shell elements. Therefore this question is still open to discussion and needs further investigations.

It is also important to notice that the differences in the stress decrease and the springback obtained by solid element between STAMP3D and DD3IMP are large. When STAMP3D was used, although the tendency in the stress decrease is different between shell and solid elements, the amount of stress decrease is relatively close. For instance, the stress decrease ranges from about 30 to 100 MPa for the initial tensile stress of 40 MPa, as shown in Fig. 3. On the other hand, when DD3IMP was used, the stress decrease was about 400 MPa and 160 MPa respectively for Swift and SKH for the initial tensile stress of 40 MPa [5]. Clearly the stress decrease is much larger for DD3IMP than those of STAMP3D. This result indicates that the amount of springback obtained by DD3IMP is much smaller. Because the same finite element type was used in the two codes, this difference may be due to other reasons other than a finite element type. This question should also be investigated in detail in order to eventually carry out accurate springback simulations.

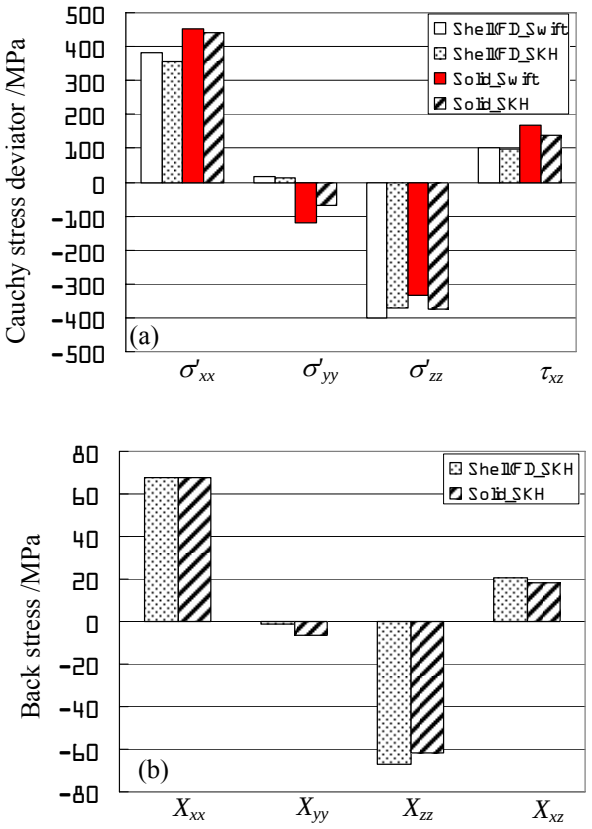

Figure 7 Stress components before springback obtained with shell element with FI and solid element for an initial tensile stress of 40 MPa. (a) Cauchy stress deviator $\boldsymbol{\sigma}'$, and (b) back stress $\boldsymbol{X}$. The subscripts *x*, *y* and *z* denote the longitudinal, width, and thickness directions, respectively.

6. CONCLUSIONS

This study focused on the effects of finite element type on springback simulation concerning the kinematic hardening. The amount of springback tends to decrease by taking kinematic hardening into account, but this trend tends to invert when the initial tensile stress gets high. This inversion arises at much lower initial tensile stress when shell element is used. Although the out-of-plane shear components are notably different between solid and shell elements, this may not be a critical factor for the above difference. This question is still open to discussion and we intend to conduct further investigations.

REFERENCES

[1] Hama T., Nagata T., Teodosiu C., Makinouchi, A., Takuda H., *Finite-Element Simulation Of Springback In Sheet Metal Forming Using Local Interpolation For Tool Surfaces*, International Journal of Mechanical Sciences, 50, 2008, pag. 175-192;

[2] Oliveira M.C., Alves J.L., Chaparro B.M., Menezes L.F., *Study on the influence of work-hardening modelling in springback prediction*, International Journal of Plasticity, 23, 2007, pag. 516-543;
[3] Lee S.W., Yang D.Y., *An Assessment Of Numerical Parameters Influencing Springback In Explicit Finite Element Analysis Of Sheet Metal Forming Process*, Journal of Materials Processing Technology, 80–81, 1998, pag. 60–67;
[4] Wagoner R.H., Li M., *Simulation Of Springback: Through-Thickness Integration*, International Journal of Plasticity, 23, 2007, pag. 345-360;
[5] Banu, M., Hama, T., Alves, J.L., and Naidim, O., *Numerical Prediction Of The Stress Fields In A Bending Unbending Forming Stage Using STAMP3D And DD3IMP*, Metal Forming Conference 2008, Steel Research International, 79, 2008, Special Edition, 1, pag. 186-193;
[6] Oliveira M.C., Alves J.L. Menezes L.F., *Algorithms And Strategies For Treatment Of Large Deformation Frictional Contact In The Numerical Simulation Of Deep Drawing Process*, Archives of Computational Methods in Engineering, 15, 2008, pag. 113-162;
[7] Banu M., Takamura M., Hama T., Naidim, O., Teodosiu, C., Makinouchi, A., *Simulation Of Springback And Wrinkling In Stamping Of A Dual Phase Steel Rail-Shape Part*, Journal of Materials Processing Technology, 173, 2006, pag. 178-184;
[8] Yamada, Y., Yoshimura, N., and Sakurai, T., *Plastic Stress-Strain Matrix And Its Application For The Solution Of Elastic-Plastic Problems By The Finite Element Method*, International Journal of Mechanical Sciences, 10, 1968, pag. 343-354;
[9] Yamamura N., Kuwabara T., Makinouchi A., *Springback Simulations For Stretch-Bending And Draw-Bending Processes Using The Static Explicit FEM Code, With An Algorithm For Cancelling Non-Equilibrated Forces*, Proceedings of NUMISHEET'02, eds, Yang D.Y., Jeju Island, 2002, pag. 25-30;
[10] Nagata T., *Simple Local Interpolation Of Surfaces Using Normal Vectors*, Computer Aided Geometric Design, 22, 2005, pag. 327-347;
[11] Hama, T., Takamura, M., Teodosiu, C., Makinouchi A, and Takuda, H., *Effect of Tool Modeling Accuracy on Sheet Metal Forming Simulation*, Key Engineering Materials, 340-341, 2007, pag. 743-748;
[12] Hama, T., Takamura, M., Makinouchi A, Teodosiu, C., and Takuda, H., *Effect of Tool Modeling Accuracy on Square Cup Deep-Drawing Simulation*, Materials Transactions, 49-2, 2008, pag. 278-283;
[13] Hama, T., Takamura, M., Makinouchi A, Teodosiu, C., and Takuda, H., *Formulation of Contact Problems in Sheet Metal Forming Simulation Using Local Interpolation for Tool Surfaces*, Journal of Computational Science and Technology, 2-1, 2008, pag. 68-80;
[14] Dvorkin, E.M., and Bathe, K.J., *A Continuum Mechanics Based Four-Node Shell Element For General Nonlinear Analysis*, Engineering Computations, 1, 1984, pag. 77-88;
[15] Bouvier S., Banu M., Maier C., Haddadi H., Teodosiu C., *18-Months Progress Report,* Inter-regional IMS contract 3DS, IMS1999000051, 2001, LPMTM-CNRS, France;